Flipper-Style Locomotion through Strong Expanding Modular Robots

Lillian Chin, Max Burns*, Gregory Xie*, and Daniela Rus

***Abstract*— Modular robotic units that can change their size at will presents an exciting pathway for modular robotics. However, current attempts have been relatively limited, requiring tethers, complex fabrication or slow cycle times. In this work, we present AuxBots: an auxetic-based approach to create high force, fast cycle time self-contained modules. By driving the auxetic shell's inherent mathematical expansion with a motor and leadscrew, these robots are capable of expanding their volume by 274% in 0.7 seconds with a maximum strength to weight ratio of 76x. These force and expansion properties enable us to use these modules in conjunction with flexible wire constraints to get shape changing behavior and independent locomotion. We demonstrate the power of this modular system by using a limited number of AuxBots to mimic the flipper-style locomotion of mudskippers and sea turtles. These structures are entirely untethered and can still move forward even as some AuxBots stall out, achieving the key modular robotics goal of versatility and robustness.**

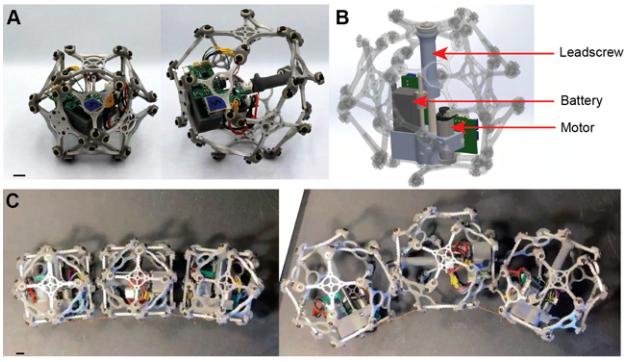

Fig. 1. (A) Overview of the auxetic robotic module in fully contracted and expanded states. (B) Computer render of the module, highlighting the internal actuation module. A motor drives the leadscrew to force the auxetic shell to expand, creating a fully untethered system. (C) The addition of wire constraints between modules not only enables bending but also allows for forward locomotion by pushing the modules against each other. Scale bars are 1 cm.

I. INTRODUCTION

Modular robotics offers a promising avenue for creating a wide range of robot topologies with versatile and robust motion. By creating systems from many identical unit robots, modular robotic systems leverage the behavior created from local deformation, achieving global shape changes [1]. However, a critical limitation for current modular robotic systems is that these dynamic movements are directly gated by how many units are part of the network. Most modular robotic systems fall under the lattice, chain or swarm architectures. If the individual robots do not change dramatically in shape, these architectures constrain large scale transformation to only occur through reconfiguration, i.e. the physical movement of n robots to another location [2].

Scaling-based systems has the potential to reduce the number of robots and traveling motions needed for large scale transformation. Rather than needing modules to move past one another like in translation / rotational-based systems [3], [4], scaling-based systems have individual units change their size directly, allowing shape change to happen in-place. This approach has strong presence in nature, such as auxesis in plant growth and morphogenesis in tissue formation [5], [6] which roboticists have drawn bioinspiration from [7]. However, current physical manifestations of this approach have had critical limitations such as complex or slow actuation, tethers to an external power source, or limited independent movement without environmental constraints [8]–[10]. We wish to develop modular systems that can leverage scaling-based approaches for untethered motion, capable of strong yet compliant actions.

In this paper, we present AuxBots, an untethered modular robotic unit that has high expansion (1.4x radius in 0.7 s) and large force capabilities (76x body mass) (Fig. 1). We extend our previous works on auxetic shells [11] to create a unit cell with controllable motor-based expansion for its single degree-of-freedom in a single robust package. The shell's movement is based on the well-understood jitterbug transformation [12], providing us with a strong mathematical basis to model our system's expansion. With this model, we can then break the traditional lattice-based architecture through the use of flexible inter-robot connections and constraints. These constraints allows the rigid AuxBots to expand past each other, enabling peristaltic motion without the need of external constraints. This combination of strength and flexiblity allows us us to mimic previously inaccessible locomotion patterns to modular robots – specifically the flipper-style movement that sea creatures like the mudskipper, sea lion and sea turtle use to move on land [13]. With only four to seven AuxBots, we are able to create untethered modular systems that can transports weights up to 19 N, even when modules stall out.

This paper makes the following contributions:

- Design and fabrication of an auxetic shell based robotic unit cell with high force and expansion capabilities
- Derivation of a mathematical model for these unit cells' single degree of freedom expansion
- Development of bioinspired flipper-style locomotion through flexible wire constraints and compliant inter-

* contributed equally with names listed alphabetically. All researchers are at the Computer Science and Artificial Intelligence Lab in the Massachusetts Institute of Technology, Cambridge, MA, USA. email: {ltchin, maxburns, gregoryx, rus}@csail.mit.edu

cell modular connections
- Demonstration of the locomotion and carrying capacity of these robots, hauling 1.5x the body mass of the system

II. BACKGROUND

Using the traditional classification schemes of modular robotics [14], scaling-based modular systems tend to follow either the lattice or swarm architectures. Traditionally, both the lattice and swarm architectures refer to modular systems where the unit modules slide or move past one another, making links where needed. This often lends these systems to primarily operate in a 2D space [15]. Since scaling-based systems can perform shape change in place, the modules often do not have actuated joints or move past one another. This can be seen dramatically in [8], where no movement occurs other than expansion and contraction of a single 2D particle in place, yet complex motion like light-following can be achieved collectively.

Although 3D volumetric expansion has been an active area of mathematical interest such as the jitterbug or Hoberman sphere [16], [17], these modules have infrequently been translated into the robotic realm and remained single, human-operated modules. The most well-known examples of scaling-based modular robotics are results from the early 2000s [14]. In [18], a rack and pinion mechanism is used to expand each side of a square outwards for reconfiguring shape changes. [19] extended this concept into 3D by using a leadscrew to drive each face of a cube outwards. While seminal, both of these works were not directly built on for hardware as the level of actuation and fabrication needed to drive this motion was prohibitively complex.

More recently, expansion-based robots has experienced a resurgence due to the popularity of soft robotics, as the fluidic-driven actuation of soft systems naturally lends itself to volumetric balloon-like expansion. Voxel-based soft simulations such as VoxCAD have fueled this interest, as these simulations assume a volumetrically expandable basis that is not currently achievable [20]. [7], [9], [10] all rely on inflation to get their volumetric expansion, only differing in their geometries and composition. [7] is most similar to the Telecubes introduced in [19] by creating silicone cubes with a magnet on each face for reconfiguring. [9] and [10] add strain limiting layers to their silicone casting, allowing for peristaltic movement and some control over friction. While these systems can achieve impressive expansion ratios, their reliance on pneumatics results in slow cycle times and a tether to an external pressure source.

III. SINGLE AUXBOT DESIGN

To make a self-contained expanding robot, we have three main goals: (1) as large an expansion ratio as possible, (2) simple untethered actuation scheme, and (3) as much force output as possible. To achieve this, we build off of our previous work of modular volumetric actuators with additional modifications to make the actuators appropriate for robotic use [11]. In this work, auxetic shells were chosen as the primary way to get expansion as their geometry simplifies expansion to a single degree of freedom problem. By rotating polygons against each other, the overall structure will follow an "auxetic trajectory", similar to Buckminster Fuller's jitterbug style expansion [17]. While novel, the actuators demonstrated in that work remained tethered to a power source and had relatively limited expansion and force capabilities (1.2x radius expansion, strength to weight ratio of 6 - 7.5x).

We improve on our previous work by designing a modular volumetric actuator with a rigid shell rather than a compliant one. Instead of bent spring steel, the faces of the auxetic pattern are now made out of 6.4 mm thick aluminum and we introduce compliance on the inter-robot level rather than the intra-robot level (Sec. V). This rigid frame offers significant advantages for performance. In the previous iteration, multiple layers of shell were needed for a sufficiently isotropic force profile. In this version, the actuation scheme is simplified by only requiring one rotating layer. This reduces unwanted joint friction and jamming caused by deformations of the shell, making the robots more isotropic by bringing the ratio of lateral to top blocked force closer to 1. The rigid shell design both improves force transmission from the unactuated to actuated faces of the robot and allows for an expansion ratio closer to the theoretical maximum of 1.7x [21], especially since there is no second layer to limit potential expansion (Fig. 2). Since the rigid faces can no longer bend to accommodate the correct dihedral constraint between faces, 3D printed joints are used (Formlabs Grey Pro, igus iglide L280). Specifically, the angle between faces must be 54.74° because the faces of the auxetic pattern lie on a cube / octahedron and thus follow octahedral symmetry [12].

To force a volumetric expansion or contraction of the shell, we can either force a rotation of antipodal points while leaving the distance between the points unconstrained by the actuator, or force the distance to change while leaving the rotation unconstrained. One of the two must remain unconstrained, since the rotation of the polygonal faces is coupled to the expansion of the shell [12]. In our previous work [11], we chose to constrain rotation to be closer to the mathematical basis of auxetic trajectories. In the interest of maximum force output, we instead choose to actuate AuxBots by controlling the distance between antipodal points, using a leadscrew as our final reduction stage. Since rotation of the faces is nonlinearly related to shell diameter (Sec. IV-A), directly controlling angle will lead to a nonlinear force profile. Controlling diameter now makes the load path from actuator to shell not go through a configuration varying reduction, making the force exerted by the robot more consistent through its range of motion. Furthermore, leadscrew reductions can generate very large output forces with small input torques with minimal component count, enabling the use of smaller motors and reducing the overall complexity of each robot. To leave the rotation of the faces unconstrained, only a single bearing needs to be added, unlike the large linear support structure needed

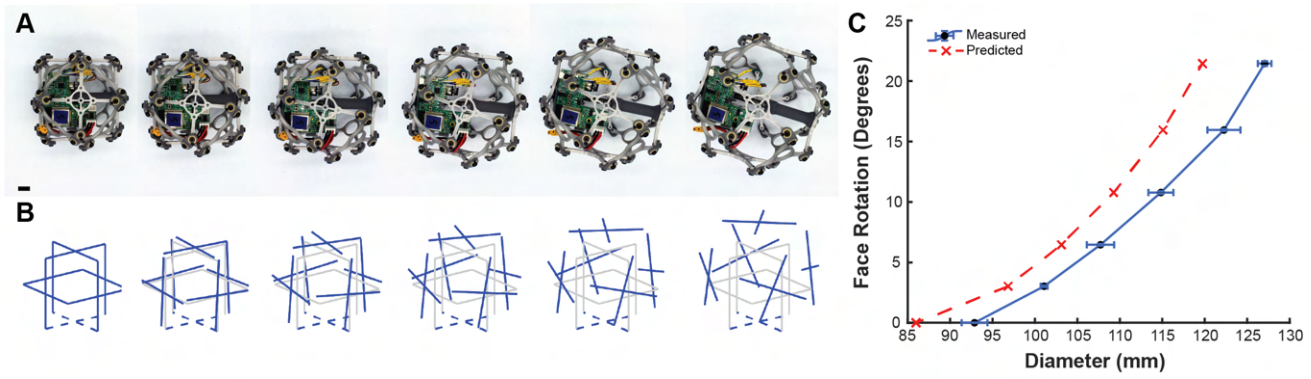

Fig. 2. (A) Top-down view of the AuxBot expanding from fully contracted to fully expanded at 7 mm increments. Scale bar is 1 cm. (B) Isometric view of the same expansion steps according to our mathematical model, tracking the square faces of the AuxBot. In our model, the bottom face (dashed line) is assumed to be fixed. The original position is shown in light gray for clarification of the expansion. (C) Measured vs. predicted values for the relationship between the AuxBot's diameter and the rotation of the top face. Prediction comes from the mathematical model of the jitterbug transformation. Error bars represent standard deviation from 3 measurements.

in [11].

The leadscrew actuation module is compact and fully integrated into the system. It is capable of exerting a force of up to 140 N with a top speed of 76.5 mm/s, all while weighing only 93 g and maintaining backdrivability. A small DC gearmotor (75:1 N20) drives a leadscrew (6mm diameter, 1.33mm pitch, 6 start), and is controlled by a microcontroller (Espressif ESP32, TI DRV8876) running a standard PI position control loop. Gains for the control loop were tuned by hand. Upon startup, each AuxBot retracts until it triggers a limit switch. This allows the AuxBot to home itself and find what position corresponds to full contraction.

The module is powered by a 8.4V 300 mAh Lithium Polymer battery. The same PCB that carries the microcontroller and motor driver also carries battery charging and protection circuitry, which allows the battery to be charged without removing it from the robot. A USB-Serial bridge allows for easy debugging and charge control. If the ESP32 detects that the current is over a set threshold for a set period of time, it will cause a software fault, protecting the AuxBot from burning out its motor. Overall, this actuation scheme is significantly simpler than comparable scaling-based robots as traditional electronics can be used to drive a single degree of freedom for all motion.

IV. SINGLE AUXBOT MODEL AND CHARACTERIZATION

A. Model of Expansion

Since each AuxBot is a cuboctahedron which expands to form a rhombicuboctahedron, we can use [12]'s method to understand the relationship between diameter to face rotation. Let $|\vec{r}| = \sqrt{r_x^2 + r_y^2 + r_z^2}$ be the radius of the overall AuxBot and our independent variable be μ, the angle of rotation between a square and triangle face. Let R_A and R_B be the radii of the circumscribing circles to the square and triangle face and $\theta_{dh} = 54.74^\circ$ be the dihedral angle constraint. Then, the radius as a function of μ

$$r_x = R_A \cos\mu$$

$$r_y = R_A \sin\mu$$

$$r_z = \frac{R_A \cos\theta_{dh}\cos\mu \pm \sqrt{R_B^2 - R_A^2 \sin^2\mu}}{\sin\theta}$$

Since we can not have self-intersection or a complex radius in the real world, we can ignore the negative branch of r_z and also know that the discriminant of r_z must be greater than 0. We also know that when the discriminant equals 0 at some μ_0, this corresponds to the "most contracted" state of the AuxBot.

In our specific case, the square and triangle faces both have sides of 45 mm and a thickness of 6.54 mm, so we know that we need to add an extra $2 \cdot 6.54 = 13.08$ mm to our predicted diameter from the equations above. We also can not measure μ but can measure the difference in rotation of the top face from its fully contracted state. To compensate for this, we subtract our measured angle from μ_0 (subtraction because of the discriminant requirement). Overall, we see a good correspondence between the physical AuxBot and the theoretical model (Fig. 2C). There is notably a consistent 5-10 mm offset between the predicted value and the measured. This is to be expected since the size of the polygons in the real AuxBot is slightly larger than the set size of 45 mm due to the added length in the dihedral constraint joints.

In addition to the general relationship between angle and expansion, we were also interested in understanding how the square faces of the AuxBot moved, as their movement would form the basis of any larger shape transformation in the bots' final lattice arrangement. We developed a set of homogeneous transformation matrices for each face of a generalized AuxBot. Let there be a coordinate axis with origin at the center of the bottom face, with the z axis pointing directly up towards the top face, the x axis perpendicular to an arbitrary side face, and the y axis perpendicular to another side face.

For a given diameter d, we let d_0 be the unactuated AuxBot's diameter, $\Delta d = d - d_0$ be the amount of diameter

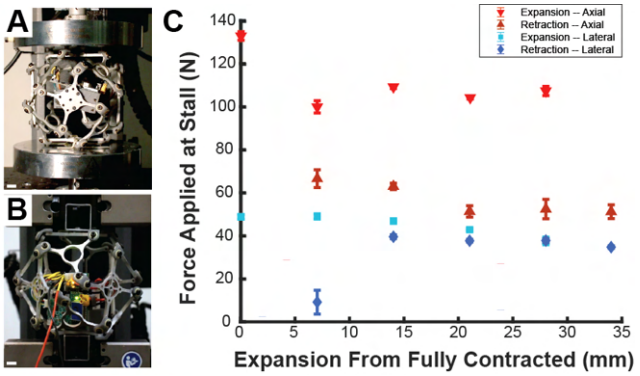

Fig. 3. Mechanical testing graph for an AuxBot's (A) expansion force and (B) retraction force. (C) The AuxBot was set at different diameters and orientations (along or lateral to the leadscrew axis) then the Instron's constraints were set to accommodate that specific diameter. The AuxBot then expanded / retracted against the Instron until the motor stalled out. Error bars represent standard deviation after 5 tests. Scale bars are 1 cm.

expansion and $\theta(d)$ be the rotation angle of each face (which can be computed via the above equations). Any point which falls upon one of the generalized robot's retracted faces can be mapped to the same point on an expanded face by compounding the following basic transformations:

1) A rotation of $\theta(d)$ about the line $x=0$, $z=d_0/2$ which passes through the center of the target face when the bot is fully retracted.
2) A translation of $\frac{\theta(d)}{2}$ away from the origin in the $-y$ direction.
3) A rotation $\theta(d)$ about the z axis.
4) A translation of $\frac{\theta(d)}{2}$ in the $+z$ direction.

As an example, here is the transform A, which takes any point on the face on the plane $y=-\frac{d_0}{2}$ to a new location on the expanded AuxBot. For legibility, let $c=\cos(\theta(d))$and $s=\sin(\theta(d))$:

$$A=\begin{bmatrix} c^2 & s & -cs & \frac{\Delta d s + d_0 cs}{2} \\ -cs & c & s^2 & \frac{\Delta d c - d_0 s^2}{2} \\ s & 0 & c & \frac{d_0+\Delta d - d_0 c}{2} \\ 0 & 0 & 0 & 1 \end{bmatrix} \quad (1)$$

B. Characterization

In addition to modeling the expansion of the AuxBot unit, we also characterized its force output and battery life of our findings can be seen in Tab. I.

To understand how long we could use the AuxBots for multi-robot applications, we conducted battery life tests by conducting expand-contract cycles with an AuxBot until the battery died. For lithium-ion battery protection, a battery is considered too low voltage to function at 7.65 V and will not respond to further commands until charged. From a maximum voltage of 8.35V, it took 1228 cycles or about 29 minutes to reach to low voltage. The actual functional time may be lower under an external load, which we were mindful in conducting experiments. There was no notable drop off in expansion ratio through this process.

TABLE I
PROPERTIES OF A SINGLE AUXBOT

Weight	180 ± 2.7 g
Closed Diameter	93 ± 1.5 mm
Open Diameter	127 ± 0.80 mm
Maximum Axially Loaded Blocked Force	135 N
Maximum Laterally Loaded Blocked Force	51.2 N
Maximum Expansion Rate	45 mm/s
Minimum Cycle Time	1540 ms
Battery Life (max cycle load)	1780 seconds, or 1230 cycles

To determine the maximum force that could be exerted by an AuxBot, we conducted mechanical tests to determine the expansion and retraction forces at varying diameters. For the expansion force, an AuxBot was ordered to a set diameter, and then secured between two flat Instron plates under slight compression (Fig. 3A). The AuxBot was then directed to fully extend until motor stall, and the maximum force was recorded for each attempt. Similarly, for the retraction force, two aluminum pieces were bolted to the top and bottom of an AuxBot, which was thens secured to the Instron in a set of tension grips (Fig. 3B). The AuxBot was then ordered to fully contract until motor stall, and the maximum force was recorded. Five tests were recorded for each diameter and loading condition, as well as along the axis of the leadscrew (axial) and perpendicular to the leadscrew (lateral).

From this characterization, we demonstrated that we successfully achieved our goals of higher force output (Fig. 3C). For a unit that only weighs 1.8 N, the AuxBot was able to exert an expansion force 23 – 76x its body weight and a retraction force 21 – 40x its body weight! Most of the variance comes from axial vs. lateral tests, with the axial expansion force nearly double the amount of force as the other modes as the leadscrew was able to take on more force. There was less variation between the lateral expansion force and the axial retraction force, when the leadscrew mattered less to the conditions. In general, the retraction force was weaker than the expansion force.

Overall, force output was fairly consistent as a function of radius, another goal of our AuxBot design. Notable outliers include the fully contracted axial expansion force, which is nearly 40 N higher than when the AuxBot is expanded by 7 mm, and the 7 mm lateral retraction force which is almost 3x less than after another 7 mm of expansion. The expansion force discrepancy may be due to the Instron directly measuring the force the leadscrew exerts on the total structure rather than what the shell as a whole exerts outward. The retraction force discrepancy is due to the compliance in the AuxBot shell. While the load path for actuator force to shell force is not configuration dependent, the load path for joint stiction to actuation force is definitely configuration dependent. Since gravity preloads the shell in an unfavorable direction for the retraction test, the actuator can move without

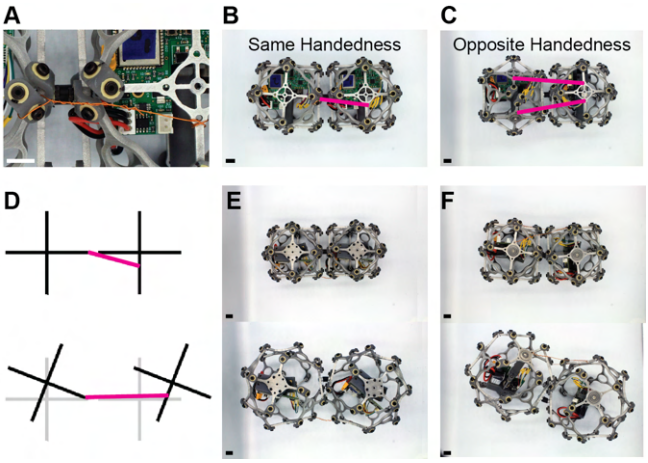

Fig. 4. (A)Wire constraints were used to induce bending by tying specific points on two AuxBots together. The effect and placement of this constraint changed depending on whether the two AuxBots had the (B) same or (C) opposite handedness, as highlighted in pink. (D) A virtual constraint was modeled to provide insight on what constraint positions would result in the most force, using length as a proxy for force. (E) This constraint led to in-plane bending for AuxBots of the same handedness (F) and off-center rotation and bending for AuxBots of opposite handedness.

moving the shell due to the slop in the joints, resulting in a lower force reading.

V. MULTIPLE AUXBOT COMPOSITION

Now that we've established the capabilities of the single AuxBot, we now turn to composing larger modular systems by connecting multiple AuxBots together. Overall, we follow the lattice architecture design, but with additional compliance in the form of soft connections and wire constraints.

To synchronously control the multi-AuxBot system, we use an offboard ESP32 to act as the server for the client ESP32 on board each AuxBot. Specifically, a Python script reads in a text file which describes a list of target diameters for each bot as a series of steps and sends these values over serial to the server ESP32. After checking that all requested diameters are within minimum and maximum diameter bounds, the server ESP32 communicates the requested expansion over the ESP-NOW protocol to all of the AuxBots. The AuxBot Client performs another check on the requested expansion ratio and uses this as the setpoint to its internal PI control loop. If one AuxBot has faulted, it will not affect the communication between the server and the other client AuxBots.

We connect adjacent AuxBots by either a rigid aluminum stand-off, or a flexible rubber disc. Flexible discs leave the relative angle between adjacent units unconstrained, while the rigid stand-offs prevent angle change or relative translation. With these basic connections alone, we can not induce locomotion as each unit will simply expand size in place – the failure mode of other scaling-based systems [8]. Rather than rely on external constraints, we choose to add wire constraints between specific positions on the faces of adjacent robots (Fig. 4A). When two robots are constrained, their expansion will change the angle formed by their center lines, creating an overall bend and potentially a slight lifting motion. This allows our modular system to move without relying on external plate or tube constraints like previous work [10], [11].

To determine the effects of wire constraint location and design the most effective connection, we extended the transform A in Eq. 1 from Sec. IV-A for two AuxBots. Two virtual robots were created, one with a bottom face centered on the origin, and the other floating with bottom face centered at $[d_0 + 10,\ 0,\ 0]$. The $+10$ offset comes from an assumed 1 cm separation between adjacent bots from the rubber disc constraint. To map points on the robot further from the origin, we define transform B. Transform B can be found by applying a translation of $\Delta d + d_0 + 10$ in the +x direction to transform A. For each of these virtual robots, query vectors were selected, $\vec{q_A}$ and $\vec{q_B}$. The distance between these vectors is subtracted from the distance between the transformed vectors as follows:

$$\Delta l = ||A\vec{q_A} - B\vec{q_B}|| - ||\vec{q_A} - \vec{q_B}|| \tag{2}$$

From this equation, we can see that Δl gives us intuition on what the most effective constraint will be (Fig 4). Since the wire constraint maintains its length under tension, a large value of Δl induces a significant change in joint angle between two robots, while a small Δl produces little effect. Constraints close to the horizontal center line of each face also produce a desirable planar force, which minimizes the out-of-plane rotation of the joint and increases stability. In practice, the model accurately represents constraint attachment schemes which minimize lifting of one robot during joint actuation.

From this proxy equation, we determine the optimal connection between two AuxBots is tying the nearest possible point on AuxBot 1 to AuxBot 2 to the hole perpendicular to the AuxBots' alignment along the centerline (Fig. 4B, D). This joint applies force largely parallel to the ground at full expansion (Fig. 4E). From experiments, this joint corresponds to a angle change of approximately 18° when both AuxBots are fully expanded.

From our experiments, we also noticed that handedness of the connected AuxBots significantly affects the performance of the joint. Each AuxBot can expand either by rotating their faces clockwise or counterclockwise. If two AuxBots of the same handedness are put together, they expand in the same way so they will not collide upon expansion. However, AuxBots of opposite handedness will expand into each other. The only way to avoid this collision is by rotating one AuxBot to be offset to the other, which is an unstable configuration (Fig. 4C, F). For our composed systems, we chose to only use AuxBots with the same clockwise orientation

VI. APPLICATIONS

With these wire constraints, we are able to use the AuxBots to perform bioinspired locomotion of flipper-based terrestrial gaits. This style of locomotion is a fairly recent

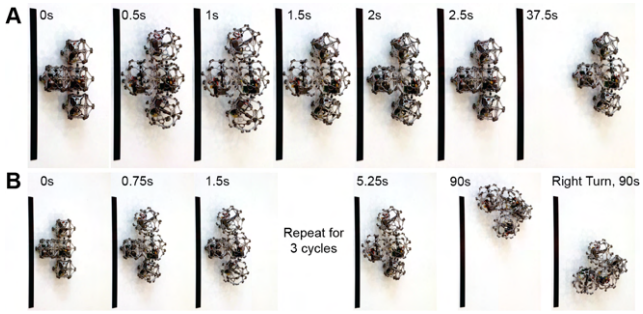

Fig. 5. Locomotion pattern for the mudskipper composition of AuxBots on posterboard. (A) Demonstration of a full cycle for moving straight with the final end state of the robot after 15 cycles. (B) Demonstration of a full cycle for turning left with the final end state of the robot after 15 cycles. The end state of the right turn experiment is also shown for completion. Scale bar is 50 cm.

area of investigation, as researchers have sought to better understand the biomechanics of motion across granular media or how to best accomodate the transition from aquatic to terrestrial environments [13], [22]. These studies have used either rigid servo chains or compliant tendon / shape memory alloy-based motion [23], so to the best of our knowledge, this is the first time modular robots have been used to mimic this style of locomotion.

We are able to do so from the AuxBot system's unique combination of strength and compliance. The wire constraints decrease reliance on the rectilinear grid which the AuxBots occupy. This allows the system to break the typical lattice assumption that other modular robots must follow through their high expansion. This gives us a lifting and bending motion that's similar to how mudskippers and sea turtles use their limbs. Furthermore, the high expansion and retraction force of the AuxBots enables them to push forward at the end of their stroke, giving a follow through to their motion pattern.

A. Mudskipper-style Locomotion

As the simplest demonstration of the composed AuxBots, we choose to mimic the mudskipper, a fish that uses its two front flippers and long tail to push itself along [24]. Similarly, we compose a set of 4 AuxBots in a T formation: two flippers on either side of a two-bot middle column (Fig. 5. The two central robots act as a torso to keep the motion stable, while the left and right joints pull the assembly forward and direct turning. Having the extra "tail" AuxBot helps to reduce sideways drift by acting as a relative anchor point to the motions of the left and right AuxBots and help the system shake free when stuck. Experiments without this fourth robot were significantly slower and more unstable. Across a felt surface, three AuxBots moved at 0.2 cm/s with a bearing of 12° while a mudskipper style design moved at 0.5 cms/s with a bearing of 7.3°. Much like their biological inspiration, the tail significantly helps the performance of the overall AuxBot system.

To move straight, we (1) expand all bots, with the middle AuxBot on a slight delay from the others, (2) contract the left and right flippers, (3) contract the tail, (4) contract the front middle AuxBot (Fig. 5A). Each cycle takes 2.5 s and gives a peristaltic wave through the system, with a slight lift and push using the flippers. For turning, we first expand all AuxBots and then repeatedly expand and contract the AuxBot on the side we wish to turn towards. This provides a pivot point for the mudskipper system to turn about. For faster turning, we have the tail AuxBot expand and contract every three open-close cycles to help propel the AuxBot forward and not just turn in place (Fig. 5B). Each cycle takes 6 seconds to complete.

TABLE II
MUDSKIPPER POSITION AFTER 15 CYCLES

Terrain	Command	Forward Distance (mm)	Sideways Distance (mm)	Bearing from Vertical (°)
Bricks	Straight	92	50	-31
	Left	118	-211	-90
	Right	250	-64	81
Carpet	Straight	242	55	11
	Left	144	47	-70
	Right	99	-54	42
Cloth	Straight	189	-21	-24
	Left	158	90	-106
	Right	102	-37	54
Concrete	Straight	92	83	-38
	Left	132	37	-60
	Right	87	-44	35
Dirt	Straight	143	-88	13
	Left	13	-3.6	7
	Right	36	-61	16
Felt	Straight	186	2.4	-7.3
	Left	155	-100	-84
	Right	102	-41	38
Posterboard	Straight	164	-4.8	-4.2
	Left	148	-51	-84
	Right	140	-28	76

Using this locomotion pattern, we conducted motion tests across several terrains, seeing how far the mudskipper AuxBot system moved over 15 cycles (Tab. II). Since turning has the additional occasional tail expansion, the actual time to perform those tests was longer than the straight movement tests (90s vs. 37.5 s). Values reported assume a coordinate axis whose origin is at the furthest back point of the tail AuxBot, with the y-axis aligned with the initial heading of the mudskipper system. Positive values represent movement to the right / clockwise of this axis while negative values represent movement to the left / counterclockwise of this axis.

Across all terrains, there is notable drifting towards moving left. This is because of our decision to make all AuxBots have the same handedness, making the overall system asymmetric. Despite this bias, the mudskipper system was still able to make right-handed turns, albeit much less effectively than making left-hand turns. The AuxBot mudskipper was able to move fastest on surfaces with moderate friction, such as the carpet and cloth. However, as friction increased, more drift and off-headings were noticed, especially in turning.

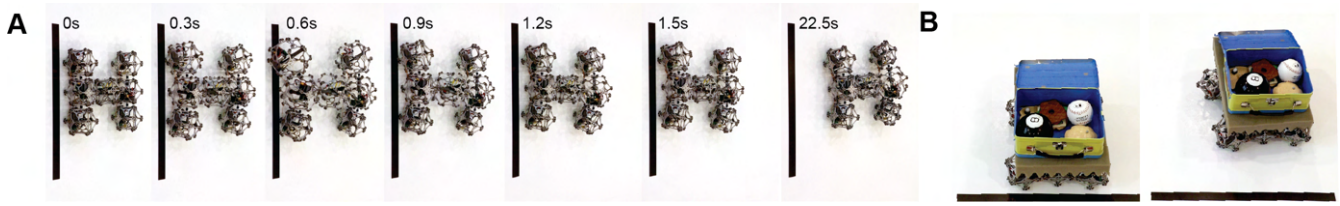

Fig. 6. Locomotion pattern for the sea turtle composition of AuxBots on posterboard. (A) Demonstration of a full cycle for moving straight with the final end state of the robot after 15 cycles. (B) Example of the AuxBots in sea turtle mode hauling weight (1027 g or 81% of system weight)

Rough terrain like dirt and grass was particularly difficult for our system, as the AuxBots would either stall or make minimal progress across the surface. Smoother surfaces like concrete made it difficult for the AuxBot to properly gain purchase on the surface and move efficiently.

B. Sea Turtle-Style Hauling

We can expand our findings from the mudskipper-style AuxBot assembly to form a stronger and stabler sea-turtle style configuration. By adding three more AuxBots to the back of the mudskipper's tail to form an I / H shape, we add redundancy and a stabler "shell" to better carry loads with. In these experiments, we used a locomotion pattern of (1) expanding all AuxBots, with a delay for the front middle and center AuxBots, (2) contracting all AuxBots except for the middle two, (3) contracting the center AuxBot, (4) contracting the front middle AuxBot (Fig. 6A). This is a generalization of the locomotion pattern for the mudskipper while leveraging the center column for more peristaltic motion. We also decreased the amount that the right-side AuxBots expanded (110 mm instead of 127 mm) in an attempt to mitigate the left drift that we saw in the mudskipper.

We test the carrying capacity of this new system by commanding the AuxBot sea turtle to move straight on posterboard while carrying a load. We laid a square of eggcrate foam on top of the AuxBots as a platform. The foam's softness helped average out all of the AuxBots' gaps and expanding motions, creating a relatively stable platform even though it was not fastened down. We then set a lunchbox on top of this foam and placed objects within there so they would not jostle off the sea turtle. Objects were placed in the lunchbox until a significant number of AuxBots stalled out, preventing further movement. Results are summarized in Tab. III.

Overall, the AuxBot sea turtle was able to carry 1938 g efficiently or about 1.5x the sea turtle's weight of 1260 g. The strength to weight ratio decrease from the individual unit characterization is largely due to the need to move while carrying a load. In order to move quickly, we oriented most of the AuxBots to be axial along the direction of movement, meaning that the weaker lateral forces are the ones that are being used to carry the object. Furthermore, from the terrain experiments, we note that the AuxBots require quite a bit of force to propel themselves forward, so additional load would affect the behavior more than just a single AuxBot expanding in place. This tracks with the overall decrease in speed and straightness we see as the load on the turtle increases. Under no load, the sea turtle moved at a similar speed to the mudskipper (4.36 mm/s vs. 4.37 mm/s), but at 1.2x loading, the sea turtle moves at 3.2 mm/s, a 25% decrease in speed. Nevertheless, the sea turtle system displays significant hauling capacity, especially considering that the higher loads (and their uneven distribution across the system) caused some AuxBots to be disabled due to motor stall. This system thus is a clear embodiment of the robustness and resilience goals of modular robotic design.

TABLE III
TURTLE POSITION AFTER 15 CYCLES (22.5 S)

Weight (g)	Forward Distance (mm)	Sideways Distance (mm)	Bearing from Vertical (°)
0	98	-3.5	-6
70	94	56	-28
447	95	64	-16
647	68	43	-7
1027	106	43	-11
1476	72	63	-18
1738*	72	-1.9	-8
1938*	64	8.9	45
2238*†	10	0.7	-5
2523*	25	-9	5
2836	4 AuxBots stalled on first expansion		

* Bottom left AuxBot stalled out after one expansion
† Middle front AuxBot stalled out after one expansion

VII. DISCUSSION

In this work, we presented a high force, large expansion, untethered robotic unit: the AuxBot. By leveraging the well-studied mathematics of the jitterbug transform, the high strength capacity of rigid robotic design, and the flexibility of compliant constraints, we were able to create modular robotic systems that could exert forces and carry loads many times their own weight. These units offer a lot of avenues for future exploration. In this work, we only considered adding wire constraints between adjacent AuxBots, but with more units, an entire line of AuxBots could be forced to curve, not just adjacent ones. In addition, sensing the load that each AuxBot feels may help lead to more efficient locomotion gaits or load balancing. This sensing could be done through external force sensors or directly by using motor current as a proxy. Overall, AuxBots represent the exciting potential of scaling-based methods for modular robotics as well as the downstream effects that soft robotics has on more effective robot designs

ACKNOWLEDGMENTS

The authors would like to thank Joaquin Giraldo-Laguna for initial prototyping, especially during the first few months of the pandemic, James Rowan for help with deriving the theoretical limit of the jitterbug transformation, and Steven Ceron for writing feedback. This work is supported by the NSF EFRI (Grant #1830901). LC is supported under the National Science Foundation Graduate Research Fellowship grant #1122374 and the Fannie and John Hertz Foundation. This article solely reflects the opinions and conclusions of its authors and not that of its sponsors.

REFERENCES

[1] J. Seo, J. Paik, and M. Yim, "Modular Reconfigurable Robotics," *Annual Review of Control, Robotics, and Autonomous Systems*, vol. 2, no. 1, pp. 63–88, 2019.

[2] H. Ahmadzadeh, E. Masehian, and M. Asadpour, "Modular Robotic Systems: Characteristics and Applications," *Journal of Intelligent & Robotic Systems*, vol. 81, no. 3-4, pp. 317–357, Mar. 2016.

[3] J. Daudelin, G. Jing, T. Tosun, M. Yim, H. Kress-Gazit, and M. Campbell, "An integrated system for perception-driven autonomy with modular robots," *Science Robotics*, vol. 3, no. 23, p. eaat4983, Oct. 2018.

[4] J. W. Romanishin, K. Gilpin, and D. Rus, "M-blocks: Momentum-driven, magnetic modular robots," in *2013 IEEE/RSJ International Conference on Intelligent Robots and Systems*. Tokyo: IEEE, Nov. 2013, pp. 4288–4295.

[5] G. K. Muday, "Auxins and Tropisms," *Journal of Plant Growth Regulation*, vol. 20, no. 3, pp. 226–243, Sep. 2001.

[6] D. M. Bryant and K. E. Mostov, "From cells to organs: Building polarized tissue," *Nature Reviews Molecular Cell Biology*, vol. 9, no. 11, pp. 887–901, Nov. 2008.

[7] A. Vergara, Y.-s. Lau, R.-F. Mendoza-Garcia, and J. C. Zagal, "Soft Modular Robotic Cubes: Toward Replicating Morphogenetic Movements of the Embryo," *PLOS ONE*, vol. 12, no. 1, p. e0169179, Jan. 2017.

[8] S. Li, R. Batra, D. Brown, H.-D. Chang, N. Ranganathan, C. Hoberman, D. Rus, and H. Lipson, "Particle robotics based on statistical mechanics of loosely coupled components," *Nature*, vol. 567, no. 7748, pp. 361–365, Mar. 2019.

[9] S. Ceron, M. A. Kimmel, A. Nilles, and K. Petersen, "Soft Robotic Oscillators With Strain-Based Coordination," *IEEE Robotics and Automation Letters*, vol. 6, no. 4, pp. 7557–7563, Oct. 2021.

[10] M. R. Devlin, B. T. Young, N. D. Naclerio, D. A. Haggerty, and E. W. Hawkes, "An untethered soft cellular robot with variable volume, friction, and unit-to-unit cohesion," in *2020 IEEE/RSJ International Conference on Intelligent Robots and Systems (IROS)*, Oct. 2020, pp. 3333–3339.

[11] J. Lipton, L. Chin, J. Miske, and D. Rus, "Modular Volumetric Actuators Using Motorized Auxetics," in *2019 IEEE/RSJ International Conference on Intelligent Robots and Systems (IROS)*, Nov. 2019, pp. 7460–7466.

[12] H. Verheyen, "The complete set of jitterbug transformers and the analysis of their motion," *Computers & Mathematics with Applications*, vol. 17, no. 1-3, pp. 203–250, 1989.

[13] N. Mazouchova, P. B. Umbanhowar, and D. I. Goldman, "Flipper-driven terrestrial locomotion of a sea turtle-inspired robot," *Bioinspiration and Biomimetics*, vol. 8, no. 2, p. 026007, Apr. 2013.

[14] L. E. Parker, D. Rus, and G. S. Sukhatme, "Multiple Mobile Robot Systems," in *Springer Handbook of Robotics*, ser. Springer Handbooks, B. Siciliano and O. Khatib, Eds. Cham: Springer International Publishing, 2016, pp. 1335–1384.

[15] Z. Butler and A. Rizzi, "Distributed and Cellular Robots," in *Springer Handbook of Robotics*, B. Siciliano and O. Khatib, Eds. Berlin, Heidelberg: Springer, 2008, pp. 911–920.

[16] R. Koppelman, "Designing an Actuated Metamorphic Mechanism based on Polyhedral Structures," Master's thesis, University of Twente, Enschede, Netherlands, 2018.

[17] E. A. Matsumoto and H. Segerman, "Geared jitterbugs," in *Proceedings of Bridges 2019: Mathematics, Art, Music, Architecture, Education, Culture*, S. Goldstine, D. McKenna, and K. Fenyvesi, Eds. Phoenix, Arizona: Tessellations Publishing, 2019, pp. 399–402.

[18] D. Rus and M. Vona, "Crystalline Robots: Self-Reconfiguration with Compressible Unit Modules," *Autonomous Robots*, vol. 10, no. 1, pp. 107–124, Jan. 2001.

[19] J. Suh, S. Homans, and M. Yim, "Telecubes: Mechanical design of a module for self-reconfigurable robotics," in *Proceedings 2002 IEEE International Conference on Robotics and Automation (Cat. No.02CH37292)*, vol. 4, May 2002, pp. 4095–4101 vol.4.

[20] J. Hiller and H. Lipson, "Dynamic Simulation of Soft Multimaterial 3D-Printed Objects," *Soft Robotics*, vol. 1, no. 1, pp. 88–101, Mar. 2014.

[21] F. Kovács, T. Tarnai, P. W. Fowler, and S. D. Guest, "A class of expandable polyhedral structures," *International Journal of Solids and Structures*, vol. 41, no. 3, pp. 1119–1137, Feb. 2004.

[22] T. Fang, Y. Zhou, S. Li, M. Xu, H. Liang, W. Li, and S. Zhang, "Theoretical and experimental study on a compliant flipper-leg during terrestrial locomotion," *Bioinspiration & Biomimetics*, vol. 11, no. 5, p. 056005, Aug. 2016.

[23] S.-H. Song, M.-S. Kim, H. Rodrigue, J.-Y. Lee, J.-E. Shim, M.-C. Kim, W.-S. Chu, and S.-H. Ahn, "Turtle mimetic soft robot with two swimming gaits," *Bioinspiration & Biomimetics*, vol. 11, no. 3, p. 036010, May 2016.

[24] C. Pace and A. Gibb, "Mudskipper pectoral fin kinematics in aquatic and terrestrial environments," *The Journal of experimental biology*, vol. 212, pp. 2279–86, Jul. 2009.